

The Long-Term Annealing of the Cluster Damage in High Resistivity n -Type Silicon

M. Kuhnke

Abstract

The annealing of the cluster damage after fast neutron and high energy π^+ -pion irradiations is studied employing the DLTS method. The clusters consist mainly of divacancies. However, other unidentified defects contribute to the signal of the single negative charge state of the divacancy. The unidentified defects are located in the cluster region. Strain and deformation fields are assumed to change the emission parameters of the defects in the cluster region resulting in a distribution of energy states. Simulations of the DLTS signals, which take into account an exponential density distribution of energy states, were carried out. During annealing a decay of divacancies and the other unidentified defects is observed.

Keywords

Silicon detectors, Radiation damage, Radiation hardness, DLTS

I. INTRODUCTION

After irradiation of silicon detectors with high energy particles the leakage current increases and the full depletion voltage changes, since the damage created in the crystal lattice changes the electrical properties of the silicon bulk [1]. During high energy particle irradiation clusters of defects and isolated point defects are produced [2]. The clusters are composed of divacancies VV and other unidentified intrinsic defects [3]. The point defects are impurity defects such as C_i , C_iC_s , C_iO_i and VO_i . After particle irradiation with small fluences used for the DLTS studies the volume generation current already dominates the reverse current, but the change in the full depletion voltage is negligible. The change in the full depletion voltage results from a change in the effective space charge density ΔN_{eff} . Recent experimental results have shown diffusion oxygenated silicon detectors to be more radiation hard in charged particle environments compared to silicon detectors processed on standard FZ silicon [4]. However, no similar beneficial effect is seen in diffusion oxygenated silicon detectors after neutron irradiation [5].

In oxygen enriched FZ the stable or time independent component of ΔN_{eff} is smaller in comparison to standard FZ after charged hadron irradiation. The beneficial effect can be explained with a decrease in the generation of the defects VP_s and V_2O [6], [7]. One assumes these defects to be generated outside the cluster regions and the generation to be affected by the content of oxygen in the silicon material [8]. The introduction rates of the two defects VP_s and V_2O are too low for detection with the DLTS method.

The component of ΔN_{eff} with a long-term annealing characteristic is named reverse annealing, because the effective space charge density becomes more negative. Reverse annealing is observed to be less damaging in oxygen enriched silicon after charged hadron irradiation. Long-term annealing is thought to be related to the annealing of the cluster damage, since the effect is not seen in ^{60}Co γ -photon irradiated samples. The reactions causing the reverse annealing are not known. A second-order reaction kinetic describes well the reverse annealing characteristic, but the time constant shows no fluence dependence as expected for a second-order process [9].

Carbon defects C_iO_i and C_iC_s are thought to form in the environment and at the periphery of the clusters [10]. The mobile carbon interstitial atoms C_i , that are produced by the exchange reaction with silicon interstitials, are attracted to the cluster region due to strain and deformation fields and captured at interstitial oxygen O_i and substitutional carbon C_s sites in the neighbourhood of the clusters. References [11], [12] suggest that an impurity-defect shell builds up during irradiation and that interstitial defects migrate from the impurity-defect shell to the cluster core during annealing. After high fluence irradiation the defect density in the impurity-defect shell is proposed to be much higher than after low fluence irradiation used for the DLTS studies. Therefore, one speculates that the defect kinetics during long-term annealing are restricted to the impurity-defect shell, which envelopes the cluster core, and the cluster core, which contains intrinsic defects, shrinks during annealing — no evaporation of interstitials from the impurity-defect shell and vacancies from the cluster core occurs, since the interstitials migrate to the cluster core and the vacancies are absorbed in the impurity-defect shell. Thus after completion of the reverse annealing processes the clusters may have a more homogeneous defect structure.

II. EXPERIMENTAL DETAILS

A sample of n -type CZ 100 Ω cm silicon, a sample of jet-oxygenated n -type FZ 800 Ω cm silicon and a sample of standard n -type FZ 120 Ω cm silicon were irradiated with Be(d,n) neutrons. The mean energy of the neutrons was 5.3 MeV. A sample of jet-oxygenated n -type FZ 800 Ω cm silicon was also irradiated with 192 MeV π^+ -pions. The effective doping concentrations are $N_{eff} = 6 \times 10^{12} - 3.5 \times 10^{13} \text{ cm}^{-3}$ and the equivalent fluences are $\Phi_{eq} = 6 \times 10^{10} - 1 \times 10^{12} \text{ cm}^{-2}$. Thus the radiation-induced defect concentrations are smaller than the effective doping concentration and the DLTS method is applicable [13]. The equivalent fluence Φ_{eq} is employed to take into account the different NIEL (Non Ionizing Energy Loss) values for Be(d,n) neutrons and 192 MeV π^+ -pions [1], [14]. The use of the NIEL to correlate radiation effects caused by different particles has already been proposed in Refs. [15], [16], [17], [18]. Simple p^+n-n^+ structures with a guard ring were processed. The exception is the CZ silicon on which a Schottky contact was evaporated. The area of the p^+ region is 5x5 mm² and the diameter of the Schottky contact is 7.5 mm. The thickness of the samples is about 300 μ m. The impurity content in the CZ 100 Ω cm material is $[O] = 9.0 \times 10^{17} \text{ cm}^{-3}$ and $[C] = 5.0 \times 10^{15} \text{ cm}^{-3}$ and in the jet-oxygenated FZ 800 Ω cm material $[O] = 1.7 \times 10^{17} \text{ cm}^{-3}$ and $[C] < 2.0 \times 10^{16} \text{ cm}^{-3}$. The standard FZ 120 Ω cm material has an impurity content of $[O] < 5.0 \times 10^{16} \text{ cm}^{-3}$ and $[C] \leq 2.0 \times 10^{16} \text{ cm}^{-3}$. A gas-jet is employed to enrich the silicon material with oxygen during the FZ process. The impurity concentrations are obtained from Secondary Ion Mass Spectroscopy (SIMS) measurements [5]. Isothermal annealing studies at 60°C were made and in some cases an additional tempering for 1280 min at 100°C.

A commercially available DLTS apparatus was employed for defect characterization that is described in more detail elsewhere [19]. Time windows of 20 ms, 200 ms and 2 s and 18 weighting functions were used to determine the emission parameters of the defects. For the simulation only the sine weighting function is used. The reverse bias was 10 V and during electrical filling with electrons a zero voltage pulse was applied to the diode. The optical filling with holes was rendered by back side illumination of the reverse biased diode with an infrared LED ($\lambda_{max} = 880 \text{ nm}$). Hence the ratio of the electron n and hole p concentrations in the space charge region was $n/p \ll 1$. Both filling pulses had a duration of 100 ms. The DLTS spectra, which correspond to the 200 ms time window and the sine weighting function (b_1 coefficient), are displayed. The capacitance (C-)DLTS technique and the constant capacitance (CC-)DLTS technique were employed to measure the capacitance or voltage transients.

III. SIMULATION DETAILS

The capacitance or voltage transients are analyzed using various weighting functions [20], [21]. The b_1 coefficient, which corresponds to the sine wave weighting function, for a discrete energy state is

calculated from

$$\begin{aligned} b_1(E_T, T) &= \frac{2 \Delta U}{T_W} \int_0^{T_W} \exp[-e_n(E_T, T) \cdot t] \cdot \sin(\omega t) dt \\ &= \frac{2 \Delta U \cdot \omega}{T_W} \cdot \frac{1 - \exp[-e_n(E_T, T) \cdot T_W]}{e_n^2(E_T, T) + \omega^2} \end{aligned} \quad (1)$$

where ΔU is the amplitude of the voltage transient, T_W the duration of the time window, E_T the energy of the defect state in the band gap, T the temperature and $\omega = 2\pi/T_W$ the angular frequency. The delay between the end of the filling pulse and the start of the transient measurement is not taken into account. The emission coefficient is

$$e_n(E_T, T) = \sigma_n \cdot v_{th,n} \cdot N_C \cdot \exp\left(-\frac{E_C - E_T}{k_B T}\right) \quad (2)$$

$$v_{th,n} = \sqrt{\frac{3 k_B T}{m_{th,n}^*}} \quad (3)$$

$$N_C = 2 \left(\frac{2 \pi \cdot m_n^* \cdot k_B T}{h^2} \right)^{3/2} \quad (4)$$

where σ_n is the cross-section, $v_{th,n}$ the thermal velocity, N_C the effective density of conduction band states, E_C the energy of the conduction band edge, k_B the Boltzmann constant and h the Planck constant. The effective thermal mass of electrons and the effective mass of conduction band state density are $m_{th,n}^* = m_n^* = 1.08 m_e$. However, a distribution of energy states alters the shape of the DLTS signal. The coefficient \tilde{b}_1 , which includes the distribution of energy states, is obtained from

$$\tilde{b}_1(T) = \int_{E_L}^{+\infty} b_1(E_T + sign \cdot E, T) \cdot D(E) dE \quad (5)$$

where $D(E)$ is the normalized density distribution of energy states. The lower integration limit E_L depends on the choice of $D(E)$, e.g. it is $E_L = 0$ for an exponential density distribution and $E_L = -\infty$ for a Gaussian density distribution. If the *sign* is positive, the energy states have a distribution towards the conduction band edge, and if the *sign* is negative, the energy states have a distribution towards the valence band edge. The defect concentration is calculated from

$$\begin{aligned} N_T &= \int_{E_L}^{+\infty} \frac{2 \varepsilon_s \cdot |\Delta U| \cdot D(E) \cdot dE}{q \cdot [(W_R - \lambda)^2 - (W_P - \lambda)^2]} \\ &= \frac{2 \varepsilon_s \cdot |\Delta U|}{q \cdot [(W_R - \lambda)^2 - (W_P - \lambda)^2]} \end{aligned} \quad (6)$$

$$\lambda = \sqrt{\frac{2 \varepsilon_s \cdot (E_F - E_T)}{q^2 \cdot n_0}} \quad (7)$$

$$E_C - E_F = k_B T \cdot \ln\left(\frac{N_C}{n_0}\right) \quad (8)$$

where ε_s is the permittivity of silicon, q the electronic charge, $W_R = \varepsilon_s/C_R$ the width of the depletion region of the reverse biased p^+n junction, $W_P = \varepsilon_s/C_P$ the width of the depletion region during application of the filling pulse, $C_{R,P}$ the corresponding capacitances per area, λ the width of the transition region, E_F the Fermi level and n_0 the free electron concentration. The introduction rate (or the fluence normalized concentration) is the defect concentration divided by the equivalent fluence.

IV. EXPERIMENTAL RESULTS

The neutron irradiated sample of jet-oxygenated FZ 800 Ω cm was first isothermal annealed to a cumulative time of 2560 min at 60°C and then tempered for 1280 min at 100°C. In Fig. 1 the DLTS spectra are shown. One notes that the annealing of interstitial carbon atoms C_i or the short-term annealing is already finished after 10 min tempering at 60°C because of the high oxygen content. An increase in the height of the signal $VO_i + C_iC_s$ and a decrease in the height of the signal $VV+?$ are

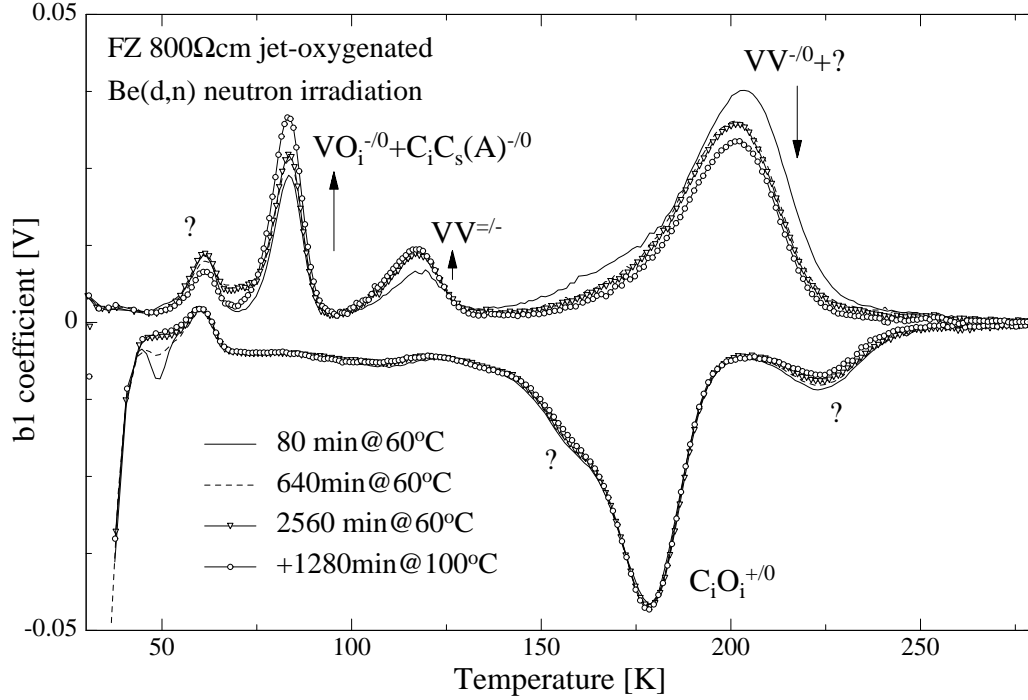


Fig. 1. The DLTS spectra of four different annealing states are shown. A change in the signals of the defects $VO_i + C_iC_s$ and $VV+?$ is observed. No change in the signal of the defect C_iO_i is visible. The various process-induced defects are labeled with question marks.

observed. However, the emission processes $VV^{-/0}$ and $VP_s^{-/0}$ arise at about the same temperature and hence the signals are superimposed. Otherwise, the generation of VP_s defects during irradiation is negligible, since the oxygen concentration is more than four orders of magnitude higher than the phosphorus concentration [6]. Hence a decay of VP_s during the 100°C tempering can be excluded. It is assumed that a decay of divacancies in the cluster regions occurs and the released vacancies are captured at O_i sites outside the cluster regions. This results in an increase in the concentration of VO_i . A release of carbon interstitial atoms C_i from the cluster regions is excluded, because the height of the signal C_iO_i is constant. The error on these data is small, since the signal of the process-induced defect on the left hand side of C_iO_i does not change. It is not very likely that both defects anneal in/out at the same rate. The constant concentration of C_iO_i indicates that no interstitial carbon atoms C_i are captured at interstitial oxygen sites O_i . The capture at C_s sites is not competitive, since the concentration of O_i sites is much higher than the concentration of C_s sites. A release of silicon interstitial atoms from the cluster regions is also excluded, since they exchange with substitutional carbon atoms $I + C_s \rightarrow C_i$. One drawback is the sum of the defect concentrations $[VO_i + C_iC_s] + 2 \cdot [VV+?]$ is not constant during annealing. However, the determination of the concentration of divacancies from the signal $VV^{-/0}+?$ may be not very reliable, when a distribution of energy states alters the shape of the DLTS signal.

In CZ silicon, which has a natural high oxygen content, the same annealing behaviour of the neutron-induced damage is observed. In Fig. 2 the dependence of the introduction rate $g(VO_i + C_iC_s)$ on the tempering time at 60°C is shown. The introduction rate is constant for tempering times

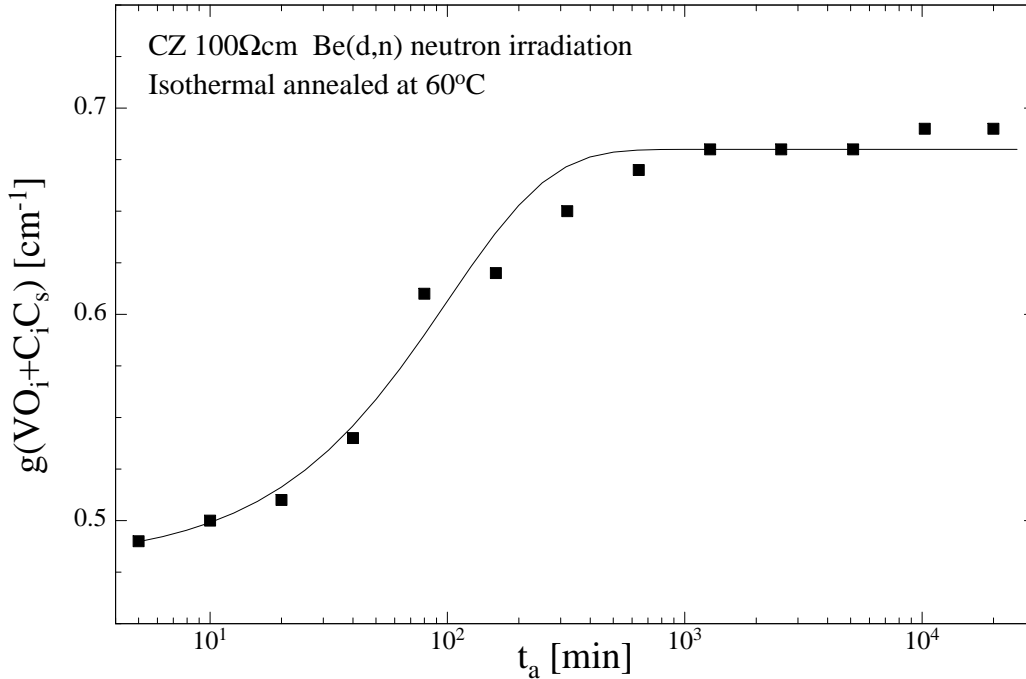


Fig. 2. The dependence of the introduction rate $g(VO_i + C_i C_s)$ on the tempering time at 60°C is shown. For tempering times $t_a > 640$ min the introduction rate is constant.

$t_a > 640$ min. This illustrates the annealing of the cluster damage or the evaporation of vacancies to be completed on this time scale. The change of the introduction rate $g(VV^+?)$ and of the ratio $[VV^=]/[VV^-+?]$ are shown in Fig. 3. One explains the difference in the concentrations of the two negative charge states of the divacancy with the bending of the electronic band structure in the cluster regions [8]. Only a fraction of the divacancies is populated with two electrons at low temperatures. The ratio $[VV^=]/[VV^-+?]$ increases with decreasing concentration of divacancies in the clusters. This observation also suggests a decay of divacancies in the cluster regions.

The DLTS signal of the divacancies concentrated in the cluster regions has been simulated. Employing an exponential density distribution of energy states the signals of the two negative charge states $VV^=$ and VV^- are calculated. Choosing a Gaussian density distribution of energy states does not reproduce the experimental data as well as an exponential one. The normalized density function is

$$D(E) = \frac{1}{\Delta E} \exp\left(-\frac{E}{\Delta E}\right). \quad (9)$$

Experimental data in Ref. [22] shows that lattice compression alters the energy states of the divacancy. Furthermore, it is assumed that the point defects C_i , $C_i C_s$, $C_i O_i$ and VO_i are located outside the cluster regions, since their emission parameters are not changed. For the calculation of the semi-infinite integral the Gaussian-Laguerre quadrature formula ($n=4$) is employed [23]. A numerical evaluation of the integral for some cases shows that the quadrature formula approximates well the integral for the used parameters. The ratio $\Delta E/(E_C - E_T)=0.04$ is kept constant. Only the ionization energy $E_C - E_T$ and the amplitude ΔU are adjusted to obtain a coincidence of the simulated and measured signals. In Fig. 4 the DLTS spectra of different annealing states together with the simulations are shown. The neutron irradiated sample of standard FZ $120\Omega\text{cm}$ was first isothermal annealed to a cumulative time of 2560 min at 60°C and then tempered for 1280 min at 100°C . The shape of the DLTS signals $VV^=$ and VV^- is material and particle independent [1], [5]. Thus it is reasonable to use a different set of DLTS spectra for the simulations. The right hand side of the signal VV^- (E4), named

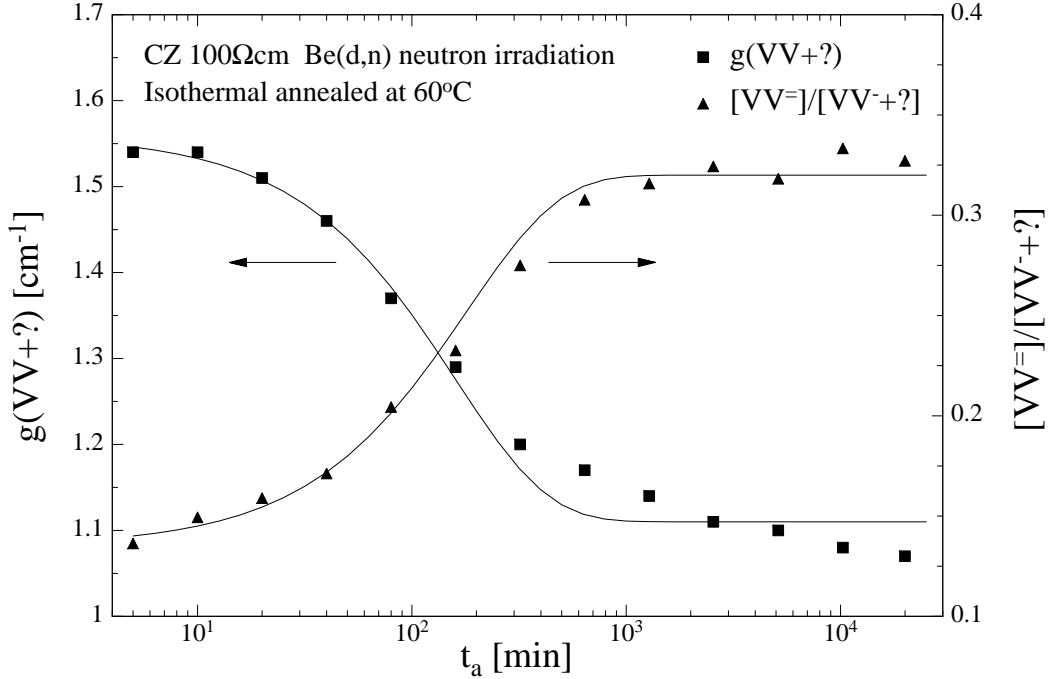


Fig. 3. The dependence of the introduction rate $g(VV^{+?})$ and of the ratio $[VV^{=}]/[VV^{-+?}]$ on the tempering time at 60°C are shown. For tempering times $t_a > 640$ min the ratio is constant.

E4b, is described reasonably by the simulation. The simulation does not fit the left hand side of the signal, named E4a. The signal E4a is assigned to an additional density distribution of energy states that is not included in the simulation. A defect identification for these energy states is not known. A multi-vacancy related defect could cause the broad signal [24]. During annealing the deviation on the

TABLE I

The parameters for which the simulation of the annealing state 80 min at 60°C has been performed are listed.

Defect center	$E_C - E_T$ [meV]	ΔE [meV]	σ_T [cm ²]	ΔU [mV]
$VV^{=}$ (E3)	250.5	+10.02	5×10^{-15}	55.0
$VV^{-+?}$ (E4)	421.5	+16.86	1×10^{-15}	209
? (E5)	500.0	-20.00	2×10^{-14}	12.0

left hand side diminishes. Another defect center with a density distribution of energy states is added to simulate the right hand tail of the signal $VV^{-/0+?}$ (E4), named E5. After the tempering period at 100°C the signal E5 is totally annealed out. Further on, the measured signal $VV^{=/-}$ (E3) shows a smaller deviation on the left hand side from the simulated signal compared to E4. Therefore the model of an exponential density distribution of energy states is more consistent with the experimental data. It is suggested that no other defect states contribute to the signal $VV^{=/-}$ (E3). In Table I the simulation parameters for the annealing state 80 min at 60°C are given. The ionization energies and cross-sections of the two charge states $VV^{=}$ and VV^{-} have the same magnitude as the ones of a single divacancy which are obtained from ⁶⁰Co γ -photon irradiated samples [8]. During annealing the decrease in the ionization energy $E_C - E_T$ of the charge state $VV^{=}$ is 4.0 meV and of the charge state VV^{-} is 7.5 meV. It is proposed that the relaxation of the lattice deformations during annealing slightly

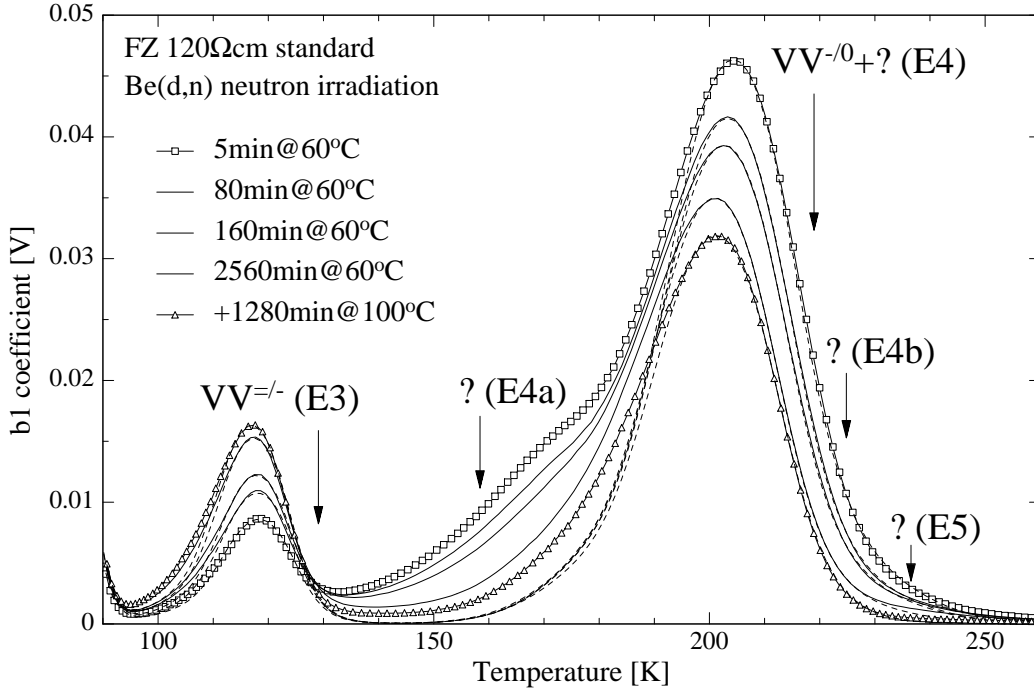


Fig. 4. The DLTS spectra of different annealing states (lines) and the simulations (dotted lines) are shown. The DLTS signals of the two negative charge states of the divacancy are simulated with an exponential density distribution of energy states.

changes the distribution of energy states. The amplitudes of the signals E4 and E5 decrease during annealing. In Fig. 5 the dependence of the introduction rates $g(E4)$ and $g(E5)$ on the tempering time is shown. The data from the sample of standard FZ 120 Ω cm irradiated with neutrons and from the sample of jet-oxygenated FZ 800 Ω cm irradiated with 192 MeV π^+ -pions are plotted. The density distribution of energy states is regarded. The experimental data clearly points up the independence of the introduction rates $g(E4)$ and $g(E5)$ on the material type. Moreover, the particle dependence is already removed by the normalization of the defect concentrations with the equivalent fluences [1]. The time dependence of $g(E4)$ is $A \cdot \exp(-t_a/\tau) + B$ with $A=0.525 \text{ cm}^{-1}$, $B=1.69 \text{ cm}^{-1}$ and $\tau=125 \text{ min}$. After tempering for 80 min at 60°C the introduction rate $g(E4)$ is higher than the introduction rate $g(VV+?) \approx 1.3 \text{ cm}^{-1}$ obtained from the DLTS spectra disregarding the distribution of energy states. For comparison the dependence of the latter introduction rate $g(VV+?)$ on the annealing time at 60°C is shown in Fig. 3. The time dependence of $g(E5)$ is $a - b \cdot \ln(t_a/t_0)$ with $a=0.196 \text{ cm}^{-1}$, $b=0.0191 \text{ cm}^{-1}$ and $t_0=1 \text{ min}$. In the sample of jet-oxygenated FZ 800 Ω cm the signal E5 cannot be simulated as well as in the sample of standard FZ 120 Ω cm, because the process-induced defect (Au_s) is assumed to contribute to the signal. The defect kinetics in the cluster regions that give rise to an exponential or logarithmic time dependence of the defect concentrations are not understood.

Since the simulation approach does not describe the left hand side of the signal $VV^{-/0}+?$ (E4), the DLTS spectra of the neutron irradiated sample of standard FZ 120 Ω cm were analyzed in the same way as the DLTS spectra of the neutron irradiated sample of CZ 100 Ω cm in Ref. [1]. The annealing of the signals E4a and E4b is studied by subtracting two interpolated DLTS spectra of different annealing states from each other. In Fig. 6 the difference DLTS spectra are shown. Two decreasing signals are revealed, also named E4a and E4b. The difference DLTS spectra indicate that the annealing of the signals E4a and E4b is completed after a tempering period for 640 min at 60°C. The emission parameters of the signal E4b determined from difference DLTS spectra of thirty-two samples are $E_C - E_T = 0.459 \pm 0.013 \text{ eV}$ and $\sigma_T = 4.50 \pm 4.26 \times 10^{-15} \text{ cm}^2$ [8]. It is noteworthy that the

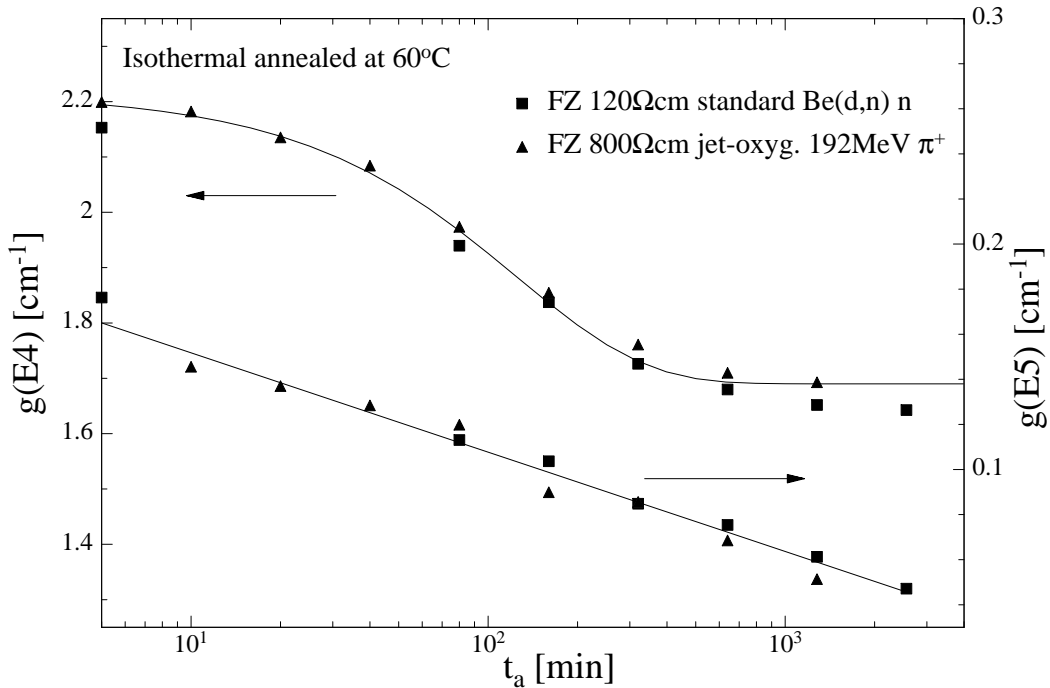


Fig. 5. The introduction rates of the cluster defects $VV^{-+?}$ (E4) and $?$ (E5) are shown (symbols). An exponential density distribution of energy states is assumed. The time dependence of $g(E4)$ is exponential and the time dependence of $g(E5)$ is logarithmic (lines).

signal E4b is well simulated assuming a Gaussian density distribution of energy states

$$D(E) = \frac{1}{\sqrt{\pi} \cdot \Delta E} \exp\left(-\frac{E^2}{\Delta E^2}\right) \quad (10)$$

with $\Delta E = 20$ meV. For this case the Gaussian-Hermite quadrature formula ($n=8$) is used to evaluate the infinite integral [23]. Furthermore, the signal E4a is regarded to be produced by a distribution of energy states around 0.36 eV. The results are in agreement with the one in Ref. [1], [25].

The location of the defects giving rise to the signals E4a, (E4b) and E5 is considered to be in the cluster regions, because the signals are only observed after particle irradiation and not after ^{60}Co γ -photon irradiation [26]. During ^{60}Co γ -photon irradiation single displacements of silicon atoms are solely created. The annealing of E4b correlates with the exponential annealing of the volume generation current [1]. On the other hand side, a correlation of the logarithmic current annealing with E5 is not possible [8].

V. CONCLUSION

The experimental results demonstrate that during the long-term annealing an evaporation of vacancies from the cluster regions occurs. The cluster damage created by fast neutrons and high energy π^+ -pions consists of divacancies and other unidentified defects. It has already been suggested that divacancies in clusters are less stable and dissociate into vacancies at lower temperatures unlike single divacancies [27]. However, a reduction in the activation energy of divacancy annealing in the presence of strain and deformation fields has been discussed and rejected in Ref. [28]. Otherwise, the dependence of the rate of divacancy annealing on the hydrostatic pressure is not known. For instance, the pressure dependence of the total change in Gibbs free energy of VP_s^0 annealing is $(\partial\Delta G_a/\partial P)_T = -10.0 \text{ \AA}^3 = -6.25 \text{ meV kbar}^{-1}$ and hence the effect is small [29]. One speculates that the elastic energy deposited into strain and deformation fields is employed to break divacancies. Moreover,

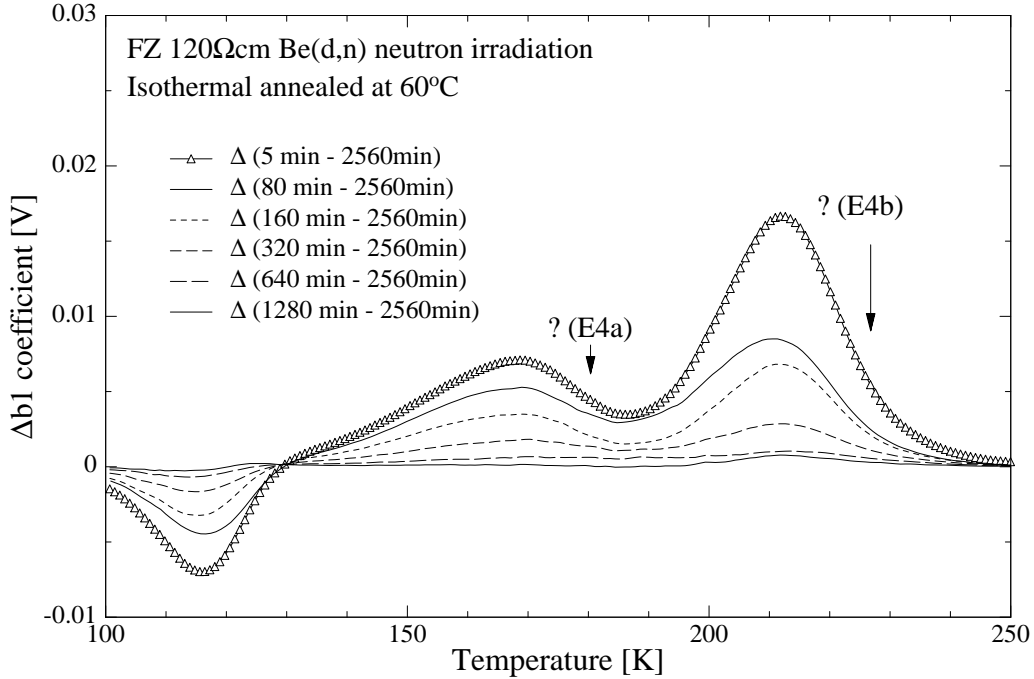


Fig. 6. The differences of interpolated DLTS spectra of two different annealing states are shown. The signals E4a and E4b vanish for tempering times $t_a > 640$ min at 60°C .

multi-vacancy complexes can release energy due to configurational changes [30]. Another conceivable annealing mechanism is the migration of interstitial defects from the impurity-defect shell to the cluster core of divacancies [28]. A decay of divacancies is also substantiated by the increase of the ratio $[VV^=]/[VV^{-/0}+?]$. The ratio $[VV^=]/[VV^{-/0}+?]$ increases with decreasing concentration of divacancies in the clusters [8]. The long-term annealing at 60°C is completed on a time scale $t_a < 640$ min.

The right hand side broadening of the signals $VV^{\pm/}$ (E3) and $VV^{-/0}+?$ (E4) can be explained with the model of an exponential density distribution of energy states. For both charge states the energy states have a distribution towards the conduction band edge. Otherwise, the left hand side broadening of the signals $VV^{\pm/}$ and $VV^{-/0}+?$ cannot be explained. The deviation of the simulation from the measured signal is less pronounced for the signal $VV^{\pm/}$ than for the signal $VV^{-/0}+?$. A distribution of energy states around 0.36 eV may cause the left hand side broadening of the signal $VV^{-/0}+?$, named E4a. A defect state at $E_C - E_T = 0.46$ eV can also reproduce the right hand side broadening of the signal $VV^{-/0}+?$, named E4b. Further on, a defect state E5 at $E_C - E_T = 0.50$ eV is added. The energy states have a distribution towards the valence band edge.

Lattice deformations are supposed to change the emission parameters of the cluster defects VV and E5. The change in the total-energy difference ΔG_n (Gibbs free energy) between two consecutive charge states depends on the pressure [31]. The isothermal pressure dependence measures a volume change. It is conjectured that $\Delta V_n = (\partial\Delta G_n/\partial P)_T$ is the volume change of the breathing-mode (symmetry-conserving) lattice relaxation (or distortion) accompanying the electron emission. For the charge state transition $VV^{\pm/}$ the enthalpy (or ionization energy) $\Delta H_n (= E_C - E_T)$ decreases at a rate of -1.2 ± 0.3 meV kbar $^{-1}$ [22]. The external applied pressure P compresses the silicon lattice. Further on, the same behaviour is expected for the charge state transition $VV^{-/0}$. Thus an estimation of the pressure within the clusters is feasible $P_{cluster} \approx 8$ kbar (for ΔE see Table I). In another way, the ionization energy of a defect charge state depends on the positions of the atoms constituting the defect. Clusters of defects can be interpreted as disordered regions and hence the atoms constituting the defects accommodate new equilibrium positions. Thus the configurational coordinates of defects inside the cluster regions

have a continuous distribution in close vicinity to the configurational coordinates of the defect species in the undisturbed silicon matrix. This effect may provide a distribution of energy states. Besides, the splitting of the energy levels due to an overlap of the wave functions of divacancies separated from each other by distances in the order of the lattice constant is also a possible explanation for a distribution of energy states [32] — the large number of clusters in an irradiated sample provides a distribution of nearest-neighbour distances resulting into an energy state distribution.

During annealing the concentration of the divacancy decreases exponentially and the concentration of the unidentified defect E5 decreases logarithmically. The annealing characteristics of defects in clusters might be due to several components [28], [30]: a relaxation of strain and deformation fields originating from the clusters accompanied by an energy release, a reduction in the activation energy of divacancy annealing in presence of strain and deformation fields, a migration of interstitial defects from the impurity-defect shell to the cluster core and an energy release from configurational changes of hypothetical multi-vacancy complexes.

VI. ACKNOWLEDGEMENTS

I would like to thank all members of the ROSE Collaboration RD48 (CERN) who make this work possible. Especially, I gratefully appreciate the assistance of R. Böttger, H.J. Brede and H. Klein during the irradiation at the Physikalisch-Technische Bundesanstalt, Braunschweig (Germany) and K. Gabathuler during the irradiation at the Paul Scherrer Institut, Villigen (Switzerland). The silicon material was provided by ITME, Warsaw (Poland) and Polovodice, Prague (Czech Republic). The processing of the diodes was done by ITE, Warsaw (Poland). Support from the European Commission contract No. ERB-FMRX-CT-980208 is greatly appreciated.

REFERENCES

- [1] M. Moll, E. Fretwurst, M. Kuhnke and G. Lindstroem, *Relation between microscopic defects and macroscopic changes in silicon detector properties after hadron irradiation*, Nucl. Instrum. Methods B, vol. 186, pp. 100–110, 2002.
- [2] V.A.J. van Lint, R.E. Leadon and J.F. Colwell, *Energy dependence of displacement effects in semiconductors*, IEEE Trans. Nucl. Sci., vol. 19, no. 6, pp. 181–185, 1972.
- [3] M. Kuhnke, E. Fretwurst and G. Lindstroem, *Defect generation in crystalline silicon irradiated with high energy particles*, Nucl. Instrum. Methods B, vol. 186, pp. 144–151, 2002.
- [4] A. Ruzin, G. Casse, M. Glasser, A. Zanet, F. Lemeilleur and S. Watts, *Comparison of radiation damage in silicon induced by proton and neutron irradiation*, IEEE Trans. Nucl. Sci., vol. 46, no. 5, pp. 1310–1313, 1999.
- [5] G. Lindström et al., *Radiation hard silicon detectors — developments by the RD48 (ROSE) collaboration*, Nucl. Instrum. Methods A, vol. 466, pp. 308–326, 2001.
- [6] B.C. MacEvoy, G. Hall and K. Gill, *Defect evolution in irradiated silicon detector material*, Nucl. Instrum. Methods A, vol. 374, pp. 12–26, 1996.
- [7] K. Gill, G. Hall and B. MacEvoy, *Bulk damage effects in irradiated silicon detectors due to clustered divacancies*, J. Appl. Phys., vol. 82, no. 1, pp. 126–136, 1997 and Erratum J. Appl. Phys., vol. 85, no. 11, pp. 7990, 1999.
- [8] M. Kuhnke, *Microscopic Investigations on Various Silicon Materials Irradiated with Different Particles with the DLTS Method*, Ph.D. thesis, DESY-Thesis-2001-009, University of Hamburg, 2001.
- [9] M. Moll, *Radiation Damage in Silicon Particle Detectors*, Ph.D. thesis, DESY-Thesis-1999-040, University of Hamburg, 1999.
- [10] M. Kuhnke, E. Fretwurst and G. Lindstroem, *The annealing of interstitial carbon atoms in high resistivity n-type silicon after proton irradiation*, Nucl. Instrum. Methods A, vol. 485, pp. 140–145, 2002.
- [11] A.V. Vasil'ev, S.A. Smagulova and S.S. Shaïmeev, *Accumulation of point defects in n-type silicon containing disordered regions*, Sov. Phys. Semicond., vol. 16, no. 1, pp. 84–85, 1982.
- [12] L.S. Smirnov, *A survey of semiconductor radiation techniques*, Mir Publishers, Moscow, 1983.
- [13] D.V. Lang, *Deep-level transient spectroscopy: A new method to characterize traps in semiconductors*, J. Appl. Phys., vol. 45, no. 7, pp. 3023–3032, 1974.
- [14] G. Lindström, M. Moll and E. Fretwurst, *Radiation hardness of silicon detectors — a challenge from high-energy physics*, Nucl. Instrum. Methods A, vol. 426, pp. 1–15, 1999.
- [15] E.A. Burke, *Energy dependence of proton-induced displacement damage in silicon*, IEEE Trans. Nucl. Sci., vol. 33, no. 6, pp. 1276–1281, 1986.
- [16] A. van Ginneken, *Non ionizing energy deposition in silicon for radiation damage studies*, Technical Report FN-222, Fermi National Accelerator Laboratory, 1989.
- [17] G.P. Summers, E.A. Burke, P.S. Messenger, S.R. Messenger and R.J. Walter, *Damage correlations in semiconductors exposed to gamma, electron and proton radiations*, IEEE Trans. Nucl. Sci., vol. 40, no. 6, pp. 1372–1379, 1993.
- [18] M. Huhtinen and P.A. Aarnio, *Pion induced displacement damage in silicon devices*, Nucl. Instrum. Methods A, vol. 335, pp. 580–582, 1993.
- [19] Dr. L. Cohausz, PhysTech GmbH, Egilbert Str. 2, D-85368 Moosburg.

- [20] S. Weiss and R. Kassing, *Deep level transient Fourier spectroscopy (DLTFS) — A technique for the analysis of deep level properties*, Solid-State Electronics, vol. 31, no. 12, pp. 1733–1742, 1988.
- [21] S. Weiss, *Halbleiteruntersuchungen mit dem DLTFS- (Deep-Level Transient Fourier Spectroscopy-) Verfahren*, Ph.D. thesis, University Kassel, 1991.
- [22] G.A. Samara, *Pressure dependence of deep electronic levels in semiconductors: Phosphorus-vacancy pair (or Si E center) and divacancy in silicon*, Phys. Rev. B, vol. 39, no. 17, pp. 12764–12774, 1989.
- [23] V.I. Krylov, *Approximate calculation of integrals*, Maximillan New York, 1962.
- [24] M. Ahmed, S.J. Watts, J. Matheson and A. Holmes-Siedle, *Deep-level transient spectroscopy studies of silicon detectors after 24 GeV proton irradiation and 1 MeV neutron irradiation*, Nucl. Instrum. Methods A, vol. 457, pp. 588–594, 2001.
- [25] S.J. Watts, J. Matheson, I.H. Hopkins-Bond, A. Holmes-Siedle, A. Mohammadzadeh and R. Pace, *A new model for generation-recombination in silicon depletion regions after neutron irradiation*, IEEE Trans. Nucl. Sci., vol. 43, no. 6, pp. 2587–2594, 1996.
- [26] M. Moll, H. Feick, E. Fretwurst, G. Lindström and C. Schütze, *Comparison of defects produced by fast neutrons and ^{60}Co gammas in high-resistivity silicon detectors using deep-level transient spectroscopy*, Nucl. Instrum. Methods A, vol. 388, pp. 335–339, 1997.
- [27] L.S. Berman, V.B. Voronkov, V.A. Kozlov and A.D. Remenyuk, *Mechanism of divacancy annealing in proton-irradiated silicon*, Sov. Phys. Semicond., vol. 26, no. 8, pp. 847–848, 1992.
- [28] I.V. Antonova, A.V. Vasil'ev, V.I. Panov and S.S. Shaïmeev, *Characteristics of annealing of divacancies in silicon containing disordered regions*, Sov. Phys. Semicond., vol. 23, no. 6, pp. 671–673, 1989.
- [29] G.A. Samara, *Breathing-mode lattice relaxation associated with the vacancy and phosphorus-vacancy-pair (E-center) defect in silicon*, Phys. Rev. B, vol. 37, no. 14, pp. 8523–8526, 1988.
- [30] J.L. Hastings, S.K. Estreicher and P.A. Fedders, *Vacancy aggregates in silicon* Phys. Rev. B, vol. 56, no. 16, pp. 10215–10220, 1997.
- [31] G.A. Samara, *Breathing-mode lattice relaxation accompanying emission and capture by deep electronic levels in silicon*, Phys. Rev. B, vol. 39, no. 15, pp. 11001–11010, 1989.
- [32] L.S. Berman, V.B. Voronkov, A.D. Remenyuk and M.G. Tolstobrov, *Energy levels of a divacancy in silicon*, Sov. Phys. Semicond., vol. 21, no. 1, pp. 84–86, 1987.